Physicochemical, morphological and thermal evaluation of lyotropic lipidic liquid crystalline nanoparticles: The effect of stimuli-responsive polymeric stabilizer

Maria Chountoulesi[a], Diego Romano Perinelli[b], Natassa Pippa[a,c], Varvara Chrysostomou[a,c], Aleksander Forys[d], Lukasz Otulakowski[d], Giulia Bonacucina[b], Barbara Trzebicka[d], Stergios Pispas[c], Costas Demetzos[a,*]

[a] Section of Pharmaceutical Technology, Department of Pharmacy, School of Health Sciences, National and Kapodistrian University of Athens, Panepistimioupolis Zografou, 15771, Athens, Greece
[b] School of Pharmacy, Via Gentile III da Varano, University of Camerino, 62032, Camerino, Italy
[c] Theoretical and Physical Chemistry Institute, National Hellenic Research Foundation, 48 Vassileos Constantinou Avenue, 11635, Athens, Greece
[d] Centre of Polymer and Carbon Materials, Polish Academy of Sciences, 34 ul. M. Curie-Skłodowskiej, Zabrze, Poland

GRAPHICAL ABSTRACT
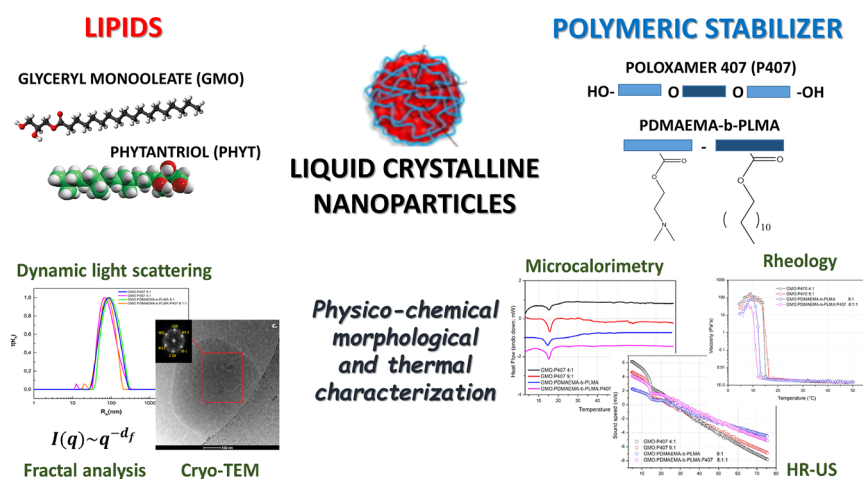
ARTICLE INFO

ABSTRACT

Non-lamellar liquid crystalline nanoparticles are promising drug delivery lipidic nanosystems, stabilized by amphiphilic block copolymers. In the present investigation, the widely used Poloxamer P407 is compared with the innovative stimuli-responsive polycationic block copolymer poly(2-(dimethylamino)ethyl methacrylate)-b-poly(lauryl methacrylate) (PDMAEMA-b-PLMA) as stabilizer for glyceryl monooleate (GMO) or phytantriol (PHYT)-based colloidal dispersions of liquid crystalline nanoparticles. As such, a variety of techniques was combined in order to comprehensively characterize these nanosystems in terms of physicochemical, morphological and thermal properties. Particle size, size distribution, ζ-potential and the fractal dimension parameter (d_f), calculated from light scattering data, as well as the morphology (from cryo-TEM analysis) of nanoparticles

* Corresponding author.
E-mail address: demetzos@pharm.uoa.gr (C. Demetzos).

were markedly affected by the different lipid and type of polymeric stabilizer, indicating different kind of interfacial lipid-polymer interactions. Notably, PDMAEMA-b-PLMA block copolymer was effective as well as P407 in stabilizing the GMO-based, but not PHYT-based nanosystems. Furthermore, microcalorimetry, high-resolution ultrasound spectroscopy and rheology were applied to characterize the thermal behavior of these nanosystems, highlighting their transition temperatures. In conclusion, a detailed evaluation was carried out on liquid crystalline nanoparticles, providing significant information, useful for the development of innovative non-lamellar therapeutic nanosystems with advanced properties that can be successfully applied in the pharmaceutical nanotechnology field.

1. Introduction

Lipid-based lyotropic liquid crystals (lamellar, cubic or hexagonal phases) represent a promising platform for the design of versatile drug delivery systems. These systems are most usually composed of glyceryl monooleate (GMO, 2,3-dihydroxypropyl oleate) or phytantriol (PHYT, 3,7,11,15-tetramethyl-1,2,3-hexadecanetriol), because these two lipids can self-assemble into different mesophases (such as cubic and hexagonal), depending on both water concentration and temperature [1–3]. These viscous bulk lipidic mesophases can be fragmentized and dispersed into non-lamellar lyotropic liquid crystalline nanoparticles, termed as cubosomes or hexosomes [1–5]. This class of lipidic nanoparticles has gained a remarkable scientific attention due to their significant advantages. More specifically, they present an increased grade of internal organisation, allowing the loading and controlled release of larger amounts of drugs and other active agents compared to liposomes, designating them as promising drug delivery nanosystems [2,4,6,7].

Lipid-based liquid crystalline nanoparticles require a stabilizer (surfactant or amphiphilic copolymer) to form stable aqueous dispersions [2,4]. In addition to the stabilizing effect, the used stabilizer can play a key role in determining the mesophases of the final nanostructures. For example, the amphiphilic PEO_{98}-PPO_{67}-PEO_{98} triblock copolymer Poloxamer 407 (P407), which is the most popular and widely used stabilizer, is proved to cause a double-diamond type (*Pn3m*) to primitive type (*Im3m*) phase transition only in GMO-prepared cubosomes, but not in PHYT-prepared cubosomes [8,9]. Therefore, the used stabilizer can be carefully designed, in order to provide extra properties [10–12], such as stimuli-responsiveness, thereby promoting a possible triggered drug release from the nanosystems exactly to the pathological tissues [13]. As such, Kluzek et al. [14] combined the P407 along with a pH-sensitive polymer, in order to develop monoolein-based cubosomes that are successfully disrupted in acidic conditions.

In the present study, we investigated a potential polymeric stabilizer, alternative to P407, and more specifically the amphiphilic block copolymer PDMAEMA-b-PLMA, consisted of the hydrophilic stimuli-responsive poly(2-(*N,N*-dimethylamino) ethyl methacrylate) (PDMAEMA) block and the hydrophobic poly(lauryl methacrylate) (PLMA) block. We also compared its stabilizing ability with the P407. PDMAEMA block, due to its functional ionizable tertiary amino group, is a weak cationic polyelectrolyte, with dual pH- and temperature-responsive properties. Tertiary amine groups of PDMAEMA blocks are fully protonated at acidic pH, promoting the cellular uptake of the nanocarrier across the negatively charged membranes of pathological tissues with lower values of environmental pH, as well as endosomal escape due to proton sponge effect [15–20]. Moreover, nanosystems based on polycationic PDMAEMA are considered to be ideal for gene delivery, thanks to their increased proton buffering capacity [16,21,22]. Additionally, PDMAEMA presents a lower critical solution temperature (LCST) in water in the range of 40–50 °C at pH 7, inducing its temperature response [18,23,24]. On the other hand, the hydrophobic PLMA block exhibits high deformability, due to its low glass transition temperature ($T_g \sim 53$ °C), along with biocompatibility [18,25].

The aim of the present study is the evaluation of an alternative polymeric stabilizer (PDMAEMA-b-PLMA) for the preparation of GMO-

and PHYT-based lyotropic lipidic liquid crystalline nanoparticles. Specifically, the physicochemical and morphological properties, as well as the thermotropic behavior of liquid crystalline dispersions stabilized by PDMAEMA-b-PLMA were investigated in comparison to the same dispersions stabilized by the commonly used P407. The systems were analysed using a gamut of techniques, as light scattering (dynamic, static and electrophoretic) for the physicochemical characterisation, cryo-TEM for the morphological evaluation, as well as microcalorimetry, high resolution ultrasonic spectroscopy and rheology for the investigation of the thermal behaviour.

To the best of our knowledge this is the first report, where lyotropic liquid crystalline nanoparticles are characterized in thermotropic terms by the aforementioned techniques, operating synergistically also with physicochemical and morphological studies. Moreover, for the first time, the fractal dimension d_f is calculated by static light scattering and proposed as a useful tool for the morphological characterisation of non-lamellar lyotropic liquid crystalline nanoparticles.

2. Materials and methods

2.1. Materials

The lipids used for the preparation of the formulations were phytantriol (PHYT, 3,7,11,15-tetramethyl-1,2,3-hexadecanetriol), which was purchased from DSM Nutritional products Ltd. (Heerlen, The Netherlands), and glyceryl monooleate Monomuls® 90-O18 [GMO, 1-(cis-9-octadecenoyl)-rac-glycerol], which was purchased from BASF (Ludwigshafen, Germany). Both lipids were used without a further purification. Differential scanning calorimetry (DSC) thermograms and ESI mass spectra of both lipids as bulk materials were also recorded, as reference (Figs. S1 and S2). The poly(2-(dimethylamino)ethylmethacrylate)-b-poly(laurylmethacrylate) (PDMAEMA-b-PLMA) amphiphilic diblock copolymer was synthesized by reversible addition-fragmentation chain transfer (RAFT) polymerization methodology, using a PDMAEMA:PLMA weight composition (%) of 69.7:30.3 [18]. The molar mass (M_w) of the diblock copolymer, as determined by size exclusion chromatography (SEC), was 9,600 g/mol and its polydispersity (PDI = M_w/M_n), as determined also by SEC, was 1.17. Pluronic® F-127 (Poloxamer P407) (PEO_{98}-PPO_{67}-PEO_{98}), with an average molar mass of 12,600 g/mol, was purchased from Sigma-Aldrich Chemical Co (St. Louis, MO, USA). All formulations were prepared in HPLC-grade water. Chloroform was of analytical grade and purchased from Sigma–Aldrich Chemical Co (St. Louis, MO, USA).

2.2. Methods

2.2.1. Preparation of liquid crystalline nanoparticle dispersions

Two different weight ratios (9:1 and 4:1) between lipid (GMO or PHYT) and P407 as stabilizer were used, corresponding to 10 % and 20 % w/w concentration of stabilizer. All liquid crystalline dispersions were prepared by using the method reported in Akhlaghi et al. [26]. Specifically, 200 mg of each lipid (PHYT or GMO) were accurately weighed into glass vials and heated at 45 °C until free flowing, following by the addition of 10 mL HPLC-grade water solution (pH = 6.0) containing the two different amounts of P407. The mixtures were

sonicated using a bath sonicator for 15 min at 45 °C, until a milky dispersion was formed, followed by two 5-min sonication cycles (amplitude 70, cycle 0.7), and interrupted by a 5-min resting period, using a probe sonicator (UP 200 S, DrHielsher GmbH, Berlin, Germany).

In the case of PDMAEMA-b-PLMA, two different ratios (Lipid:PDMAEMA-b-PLMA 9:1 and Lipid:PDMAEMA-b-PLMA:P407 8:1:1) were used, corresponding to 10 % and 20 % w/w concentration of total stabilizer relative to the lipid mass. In particular, 200 mg of each lipid were fully dissolved in chloroform, while PDMAEMA-b-PLMA block copolymer was fully dissolved in chloroform:methanol 9:1 (5 mg/mL w/v). Dissolved lipid and block copolymer were mixed in appropriate amounts and the solvent was slowly removed at 45 °C under vacuum (Rotavapor R-114, Buchi, Switzerland) until a thin lipidic film formed. The prepared film was hydrated with 10 mL of HPLC-grade water (pH = 6.0), containing also dissolved the P407 in the cases of 8:1:1 systems. In the case of PDMAEMA-b-PLMA, a supplementary drop-wise acidification with hydrochloric acid 1 N to pH = 3.0 was required in order to efficiently stabilize the GMO:PDMAEMA-b-PLMA 9:1 system. Subsequently, the mixtures were sonicated using a bath sonicator for 30 min, at 45 °C until a milky dispersion was formed, followed by three 5-min sonication cycles (amplitude 70, cycle 0.7), and interrupted by 5-min resting periods, using an ultrasonicator (UP 200 S, DrHielsher GmbH, Berlin, Germany).

The eight resultant dispersions were allowed to anneal for 30 min and then transferred into vials and stored at room temperature. The lipid concentration was 20 mg/mL in all prepared dispersions. The temperature used for the preparation process (45 °C) was chosen to obtain dispersions, according to the phase diagrams of each lipid in water. Temperatures higher than 50 °C were avoided, in order not to overtake the LCST of the PDMAEMA.

2.2.2. Physicochemical and Morphological Characterization of the liquid crystalline nanoparticles

2.2.2.1. Dynamic (DLS) and Static (SLS) light scattering measurements.
Dynamic and static light scattering measurements were performed using an AVL/CGS-3 Compact Goniometer System (ALV GmbH, Germany), equipped with a cylindrical JDS Uniphase 22 mV He–Ne laser, operating at 632.8 nm, and an Avalanche photodiode detector. The system was interfaced with an ALV/LSE-5003 electronics unit, for stepper motor drive and limit switch control and an ALV-5000/EPP multi-tau digital correlator. For light scattering measurements, 100 μL of aliquots were diluted 30-fold in HPLC-grade water (pH = 6.0) and then analyzed. The hydrodynamic radius (R_h) and the size polydispersity index (*PDI*) of the prepared nanosystems were obtained from DLS technique. Autocorrelation functions were analyzed by the cumulants method and the CONTIN software. Apparent hydrodynamic radius, R_h, at finite concentrations was calculated by the Stokes–Einstein equation:

$$R_h = \frac{k_B T}{6\pi n_0 D}$$ (1)

Where, k_B is the Boltzmann constant, n_0 is the viscosity of water at temperature T, and D is the diffusion coefficient at a fixed concentration. The polydispersity of the particle sizes was given as the μ_2/Γ^2 (PDI) from the cumulants method, where Γ is the average relaxation rate, and μ_2 is its second moment.

SLS has been used to determine the fractal dimensions of aggregates. A beam of light is directed into a sample and the scattered intensity is measured as a function of the magnitude of the scattering vector q, with:

$$q = \frac{4\pi n_0}{\lambda_0} \sin\frac{\theta}{2}$$ (2)

Where, n_0 is the refractive index of the dispersion medium, θ is the scattering angle and λ_0 is the wavelength of the incident light. Measurements were made at the angular range of 30-150° (*i.e.* the range

of the wave vector was $0.01 < q < 0.03$ cm^{-1}).

The general relation for the angular dependence of the scattered intensity, $I(q)$ is:

$$I(q) \sim q^{-d_f}$$ (3)

Where, d_f is the fractal dimension of the nanoparticles or aggregates with $1 \le d_f \le 3$ ($d_f = 3$ corresponds to the limit of a completely compact Euclidean sphere where less compact structures are characterized by lower d_f values). The above equation was used to determine the mass fractal dimension from the negative slope of the linear region of a log-log plot of I vs q. For evaluating the temperature dependency of the d_f, each SLS measurement was carried out at two temperatures (25 °C and 55 °C), using a temperature controlled circulating bath (model 9102 from Polyscience, USA) connected to the measuring cell of the light scattering instrument. An additional measurement was then carried out at 25 °C again after cooling. Equilibration times of 15 min were utilized between measurements at different temperatures [27–30]. The effect of the acid pH of the medium in the d_f of the PDMAEMA-b-PLMA systems was investigated by diluting 100 μL of aliquots 30-fold in Citrate Buffer with pH = 4.2. The samples were incubated at room temperature for 20 min and the SLS measurements were repeated as described.

2.2.2.2. Electrophoretic light scattering (ELS).
The ζ-potential (ζ-pot, mV) of the prepared nanosystems was measured through electrophoretic light scattering (ELS). 100 μL of aliquots were diluted 30-fold in HPLC-grade water (pH = 6.0). The protocol of ELS measurement is described in detail in our previous reports [27–30].

2.2.2.3. Cryogenic Transmission Electron Microscopy (Cryo-TEM).
Cryogenic transmission electron microscopy (Cryo-TEM) micrographs were obtained using a Tecnai F20 X TWIN microscope (FEI Company, USA) equipped with a field emission gun, operating at an accelerating voltage of 200 kV. Images were recorded on the Eagle 4 k HS camera (FEI Company, USA) and processed with TIA software (FEI Company, USA). Specimen preparation was done by vitrification of the aqueous (HPLC-grade water) solutions on grids with holey carbon film (Quantifoil R 2/2; Quantifoil Micro Tools GmbH, Germany). Prior to use, the grids were activated for 15 s in oxygen plasma using a Femto plasma cleaner (Diener Electronic, Germany). Cryo-samples were prepared by applying a droplet (3 μL) of the solution to the grid, blotting with filter paper and immediate freezing in liquid ethane using a fully automated blotting device Vitrobot Mark IV (FEI Company, USA). After preparation, the vitrified specimens were kept under liquid nitrogen until they were inserted into a cryo-TEM-holder Gatan 626 (Gatan Inc., USA) and analyzed in the TEM at −178 °C. Pictures were processed using ImageJ software.

2.2.3. Characterization of thermal behavior of dispersions

2.2.3.1. Microcalorimetry (mDSC).
0.750 g of the sample and an equal amount of water as reference were filled in Hallostey calorimetric cells and equilibrated at 5 °C for 20 min. Then, a heating and a cooling ramp in the temperature range from 5 °C to 80 °C, at 1 °C /min rate, were performed. Calorimetric analyses were carried out using a microDSC III (Setaram, France). The temperature (Tm, °C) and enthalpy (ΔH, J/g of solution) were calculated from the peak and the area of the transition using the software of the instrument (Setsoft 2000, Setaram) according to the tangent method. All measurements were performed in triplicates.

2.2.3.2. High-resolution ultrasound spectroscopy.
Differential relative ultrasonic velocity and attenuation for samples were recorded as a function of temperature using a HR-US 102 high-resolution spectrometer (Ultrasonic Scientific, Ireland) at the frequency of 5.4 MHz, preliminarily determined by a broad amplitude frequency scan. Around 2 mL of samples and reference (water) were filled in the ultrasonic cells and left at 5 °C for at least 20 min for temperature equilibration and, then, subject to the same thermal programme used

for mDSC analyses (from 5 °C to 80 °C at 1 °C/min). Temperature was controlled using a HAAKE C25 P thermostat (Thermo Electron Corporation, Germany). Ultrasonic attenuation and sound speed are reported as differential values, obtained by subtracting the contribution of the reference from the value recorded in the sample cell. Sample transitions were calculated from the first-derivate of the signal in the case of sound speed. All measurements were performed in triplicate.

2.2.3.3. Rheological analysis. Rheological analyses were performed using a rotational rheometer (Kinexus Lab +, Malvern, UK), equipped with a cone-plate (C 40/4) geometry.

A Viscometry test at a constant stress of 0.1 Pa was performed in the range of temperature 5 °C–50 °C. Viscosity (Pa*s) of the systems were recorded with a step of 1 °C after 2 min of equilibration at each temperature. The transition temperature was calculated using a nonlinear regression model (Prism version 5.0, GraphPad Inc., USA) as follows:

$$Y = \text{BOTTOM} + \frac{\text{Top} - \text{Bottom}}{1 + 10^{(\text{Log T} - x) \, \text{Hill Slope}}} \tag{4}$$

Where, Top and Bottom are plateaux in the units of the Y axis and T is the transition temperature.

3. Results and discussion

3.1. The physicochemical and morphological characteristics of the liquid crystalline nanosystems as revealed by DLS, ELS and cryo-TEM

The different lipid (GMO and PHYT), and the polymeric stabilizer (P407 and PDMAEMA-b-PLMA) (Fig. 1) affected the size, as well as the morphology of the resultant nanosystems. Regarding the used lipid, the four PHYT-based nanosystems presented larger average size (R_h) values than the GMO respective ones (Table 1). Apart from the larger R_h, the systems with PHYT lipid were less homogeneous, exhibiting larger values of PDI, as well as broader size distribution traces (Fig. 2). Furthermore, it can be seen that the increase of the total amount of the polymeric stabilizer (from 9:1 to 4:1 w/w) led to a decrease of the particle size, probably due to a larger degree of reduction of the interfacial tension between the lipid and the water phases. We should mention that the polymeric concentration plays a key role regarding the physicochemical and morphological characteristics of nanosystems. The increase of the polymeric concentration can not only reduce the nanoparticle size, but also increase the amount of vesicular structures [8,11]. In particular, a formulation of lipid:polymer 4:1 w/w contains a very high amount of polymers, which may form micelles or promote lipid vesicle formation due to the excess polymers in the system. More analytically, as literature describes, at high stabilizer concentrations, the lipid can be solubilized into the formed mixed lipid-polymer micelles, or even can form vesicular structures, such as liposomes, reducing the percentage of the presenting cubic structures [11,26]. These literature results related to the effect of the polymeric concentration into the morphology, are also in accordance with our cryo-TEM results, being described below.

The polymeric stabilizer was also proved to be a crucial parameter for the ζ-potential of the nanosystems (Table 1). The systems containing P407 as exclusive stabilizer presented high negative values of ζ-potential, probably due to the PEO block of P407 covering the external surface of the nanoparticles and absorbing hydroxyl anions from the aqueous medium [31]. In contrast, the replacement of P407 with PDMAEMA-b-PLMA caused a conversion of ζ-potential values from negative to high positive values, owing to the charged tertiary amino groups of PDMAEMA block, which are protonated in the pH of the medium (pH = 6.0, or lower due to the acidification required in the GMO:PDMAEMA-b-PLMA 9:1). The combination of the two stabilizers (8:1:1 systems) produces medium positive values of ζ-potential, especially in the case of GMO-based system. Maybe the longer PEO block of P407 can partially shield the charged groups of PDMAEMA.

Although at the preparation day the four PHYT systems presented similar physicochemical characteristics, throughout their first week after their preparation the two PHYT systems with PDMAEMA-b-PLMA showed some permanent aggregates, which were not redispersed by hand shaking, reflecting a partial phase separation. Among the PHYT systems, the P407 copolymer was proved to be much more efficient stabilizer than the PDMAEMA-b-PLMA copolymer, since the two PHYT:P407 colloidal dispersions were stable over 40 days after their preparation (Fig. S3). We should note that due to their rapid collapse, we chose not to go on with further characterizations of the two PHYT systems prepared with PDMAEMA.

Differently to PHYT:PDMAEMA-b-PLMA systems, the four GMO dispersions were proved to be stable over time, exhibiting no significant difference in R_h and PDI values for at least a period of 90 days (Fig. S4). However, we should note that the PDMAEMA-b-PLMA required a supplementary drop-wise acidification with hydrochloric acid, apart from the sonication process, in order to efficiently stabilize the GMO:PDMAEMA-b-PLMA 9:1, while the P407 stabilized the remaining three GMO systems without acidification, as well as requiring less time of bath and probe sonication.
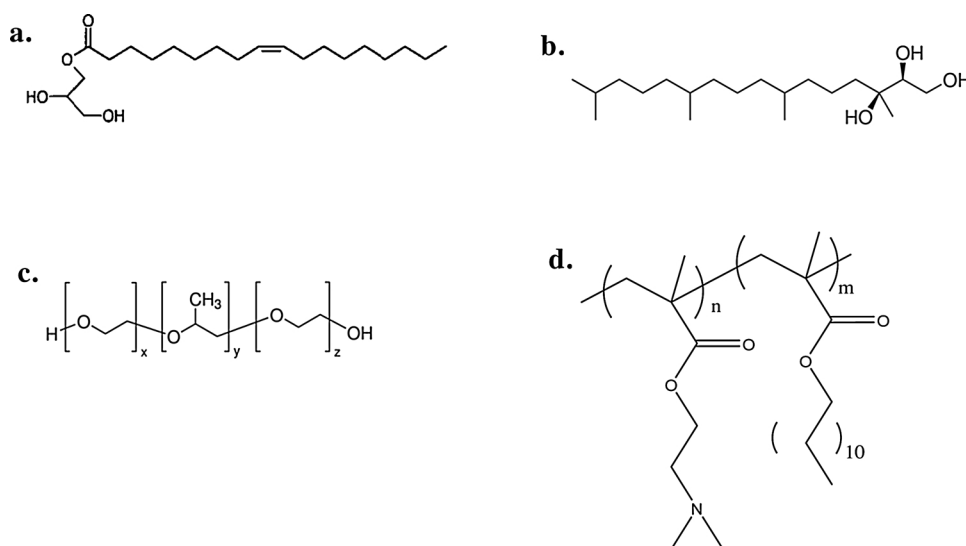

Fig. 1. Chemical structures of GMO (**a**) and PHYT (**b**) lipids, and polymeric stabilizers Poloxamer P407 (PEO$_{98}$-PPO$_{67}$-PEO$_{98}$) (**c**) and PDMAEMA-b-PLMA (**d**), employed in this study for the formulation of lyotropic liquid crystalline nanoparticles.

Table 1
Physicochemical properties (hydrodynamic radius, R_h; polydispersity index, PDI and zeta potential, ζ-pot) of the nanosystems prepared in HPLC grade water measured during the preparation day (t = 0 days). Data are reported as mean values ± standard deviations of triplicate measurements.

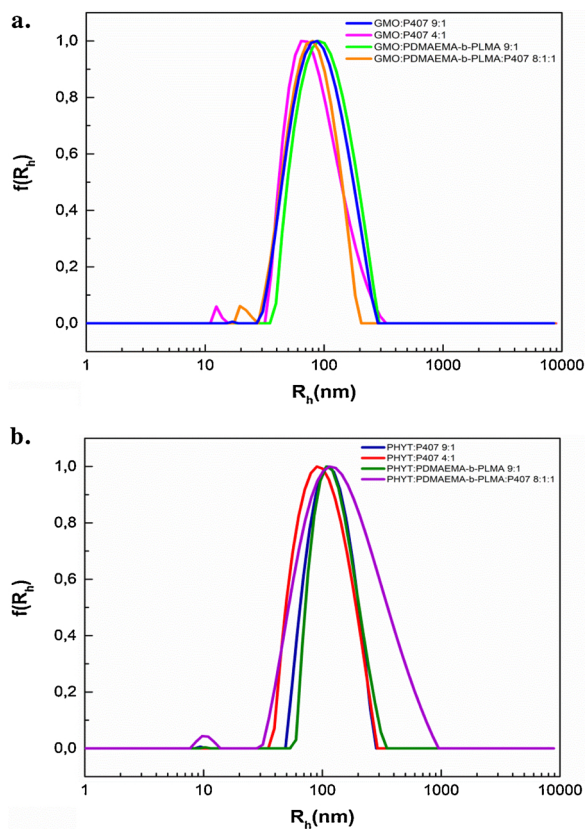| Sample	Weight ratio	R_h (nm)	PDI	ζ-pot (mV)
PHYT:P407	9:1	148.7 ± 2.1	0.361 ± 0.098	−21.3 ± 2.1
PHYT:P407	4:1	109.6 ± 2.6	0.364 ± 0.056	−20.7 ± 1.5
GMO:P407	9:1	74.3 ± 1.2	0.286 ± 0.013	−30.2 ± 3.2
GMO:P407	4:1	72.3 ± 1.8	0.250 ± 0.010	−30.5 ± 1.2
PHYT:PDMAEMA-b-PLMA	9:1	120.1 ± 2.3	0.326 ± 0.016	21.4 ± 0.5
PHYT:PDMAEMA-b-PLMA:P407	8:1:1	112.3 ± 1.5	0.588 ± 0.021	21.3 ± 2.0
GMO:PDMAEMA-b-PLMA	9:1	88.9 ± 2.4	0.331 ± 0.014	52.5 ± 1.8
GMO:PDMAEMA-b-PLMA:P407	8:1:1	76.7 ± 1.5	0.270 ± 0.013	19.3 ± 1.5

Fig. 2. Particle Size distributions (R_h) from dynamic light scattering (DLS) of GMO- (**a**) and PHYT- (**b**) based nanosystems.

The different interactions between the different lipids and polymeric stabilizers can explain the above physicochemical observations. Literature confirms that the methyl groups of PPO block of the P407 exhibit an unfavourable steric interaction with the branching structure on the hydrocarbon chain of the PHYT lipid, decreasing P407 affinity for the PHYT. Consequently, a lesser extent of P407 adsorption on PHYT-based particle surface occurs when compared to GMO [9,31], which can explain the size and size distribution differences between GMO and PHYT-based systems. Moreover, it can be hypothesized that similar phenomena of reduced affinity may be produced also by the methyl groups of the PLMA block, leading eventually to the observed rapid phase separation of the two PHYT-based systems containing PDMAEMA-b-PLMA.

According to cryo-TEM results, the GMO-based systems showed also a different kind of morphology, compared to PHYT-based ones. Starting from those containing P407 as exclusive stabilizer, we observed a morphological variety existing in the GMO based dispersions for both 9:1 and 4:1 ratios (Fig. 3a, b), as it has been also pointed out by Barauskas et al. [32]. More specifically, we observed different sized structures including simple vesicles, exhibiting no internal structure (Fig. 3a, b, red arrows) along with more intricate, liquid crystalline confined nanoparticles, exhibiting regularly (Fig. 3a, b, blue arrows) or less periodical, irregularly ordered structure (Fig. 3a, b, yellow arrows). The yellow arrows maybe show some "sponge"-like surface structures (L_3), while the blue arrows present square-shaped motifs resembling to cubic phases. The corresponding Fast Fourier Transform (FFT) pattern of the red box area (inset in Fig. S5) of the GMO:P407 9:1 system is likely corresponding to cubic structure of *Im3m* symmetry [32], being in agreement with the literature, denoting that the P407 causes a double-diamond type (*Pn3m*) to primitive type (*Im3m*) phase transition in GMO-prepared cubosomes [8,9]. In Fig. 3b, the black arrow points out a fusion process between vesicles which probably illustrates a premature step towards the dynamic formation of liquid crystalline nanoparticles. Moreover, we observed an intermediate structure of intersecting lamellas that cannot be classified at none of the above categories, pointed by green arrow in Fig. 3a. This structure simulates the "spider's web" and maybe reflects another pre-stage of organization degree, after the vesicles and before the liquid crystalline nanoparticles.

From the morphological point of view, the two PHYT:P407 systems presented nanoparticles, with striated, regularly ordered inner structure as illustrated by cryo-TEM images (Figs. 3c, d, S6, S7). The corresponding Fast Fourier Transform (FFT) patterns of red box areas (insets in Figs. 3c, d and S6) are likely with cubic structure of *Pn3m* symmetry [33]. According to Dong et al. [9], the P407, being simply absorbed in the surface and not inserted into the PHYT bilayer, does not cause a double-diamond type (*Pn3m*) to primitive type (*Im3m*) phase transition, as in the case of GMO cubosomes. Apart from individual nanoparticles (Fig. 3c), some of them create also aggregates (Fig. 3d) up to 2 μm. A noteworthy difference, in comparison to the GMO:P407 systems, is the absence of other intermediate or vesicular structures, neither dispersed, nor attached to the surface of the liquid crystalline particles.

The replacement of P407 with PDMAEMA-b-PLMA resulted in the predominance of fusion phenomena in GMO-based systems (Fig. 4a, b). There are different combinational structures, such as liquid crystalline nanoparticles either being between two vesicles (Fig. 4a, b blue and purple arrows) or attached to one vesicle (Fig. 4a, green arrow). There are also sponge-like structures attached to vesicles (Fig. 4a, yellow arrow). Vesicular structures exist either alone or fusing with other vesicles (Fig. 4a, b red arrows). In contrast, the combination of the two polymers at the same weight ratio (GMO:PDMAEMA-b-PLMA:P407 8:1:1) yields an increase of the lipid organization towards to confined, regularly ordered liquid crystalline nanoparticles (Figs. 4d, S8, blue arrow). A large surface of aggregated nanoparticles, dispersed with a multitudinous and multi-shaped population of empty vesicles was also observed (Fig. 4c). The internal structure of the red box area of this organized phase (Fig. 4c), assessed by the Fast Fourier Transform (FFT), is likely with cubic structure of *Pn3m* symmetry [33].

The vesicular structures co-dispersed with nanoparticles, being observed at the four GMO systems (independently from the stabilizer), are supposed to act as a further stabilization factor of the cubic phases. The vesicles that are attached to the nanoparticles surface create a
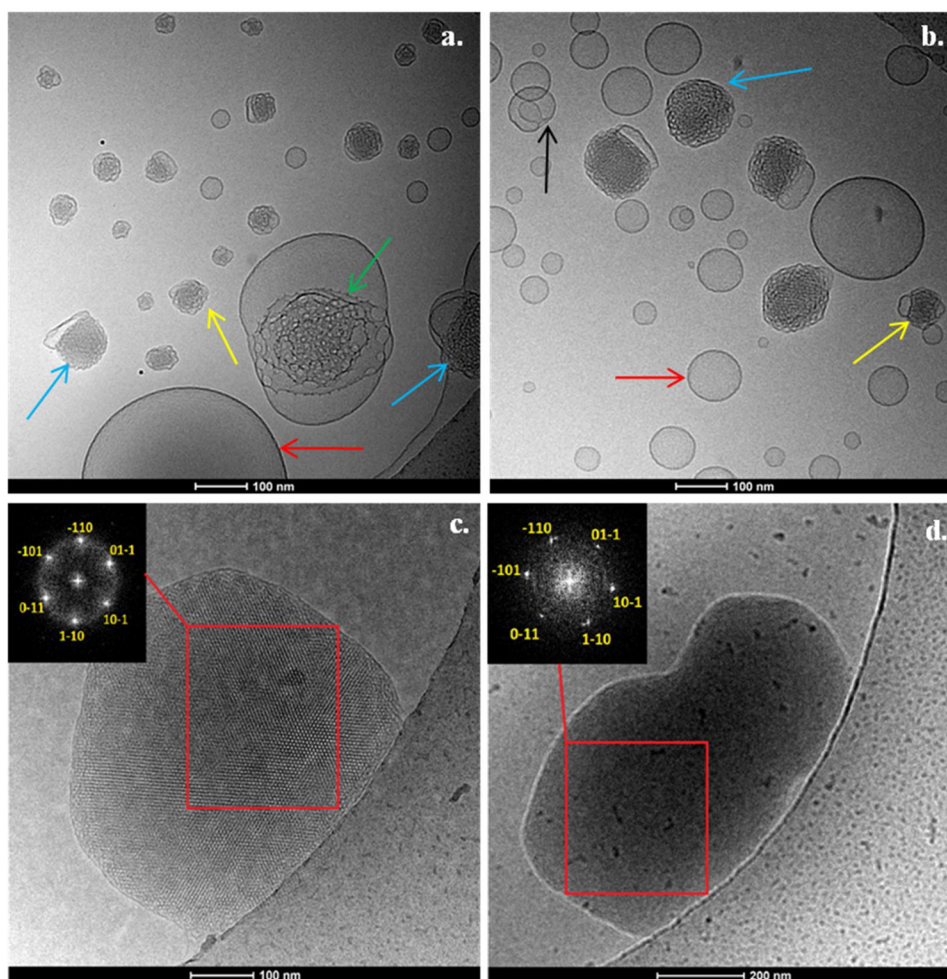
Fig. 3. Cryo-TEM images from GMO:P407 9:1 (**a**), GMO:P407 4:1 (**b**), PHYT:P407 9:1 (**c**) and PHYT:P407 4:1 (**d**) nanosystems. The corresponding Fast Fourier Transform (FFT) patterns of red box areas (insets in images **c** and **d**) are likely with cubic structure of *Pn3m* symmetry. (For interpretation of the references to colour in this figure legend, the reader is referred to the web version of this article).

protective coating layer that can prevent nanoparticle aggregation and keep the nanoparticles in dispersion [8,32]. By comparing Figs. 3a and b with 4 a and b, we should mention that all the organized nanoparticles, being observed in GMO:PDMAEMA-b-PLMA 9:1 system, are agglutinated to one or more vesicles, presenting the motif of combinational structure, in contrast to the two GMO:P407 systems, which contained some individual nanoparticles of larger sizes (Fig. 3a and b, blue arrows). Comparing 4:1 and 9:1 ratios of GMO:P407 systems, a greater number of vesicles was numerated at 4:1 ratio due to the increase of stabilizer amount [8,11]. Thus, the different polymeric stabilizer, as well as its concentration, can play a crucial role on the organization and the diversity of the morphological characteristics of the liquid crystalline nanostructures.

Finally, by taking into account our experimental observations during the preparation process, as well as the physical stability of the systems, we can also compare the stabilizing ability of the two polymers utilized. Literature describes that higher hydrophilic-to-hydrophobic ratio of the copolymer can promote a more efficient stabilization, because the longer hydrophilic polymeric block creates a greater entropic effect [34,35]. Probably due to the longer PEO block, PHYT:P407 systems were stabilized for a longer time, compared to the case of the shorter one PDMAEMA block. Regarding the GMO systems, P407 was proved also more efficient stabilizer, while PDMAEMA-b-PLMA stabilized the systems either as a co-stabilizer with P407 (GMO:PDMAEMA-b-PLMA:P407 8:1:1) or individually with acidification (GMO:PD-MAEMA-b-PLMA 9:1). The acidification probably increased the

hydrophilicity of the PDMAEMA block, due to a higher protonation degree of its amino groups.

3.2. Fractal analysis of the liquid crystalline nanosystems

In addition to cryo-TEM, static light scattering (SLS) can provide through fractal analysis useful *in situ* information about the structure of colloidal nanoparticles in real conditions and in dispersion state [36,37]. The fractal dimension (d_f) represents a parameter of the quantification of the morphology and has already been estimated for other colloidal nanostructures, such as liposomes, dendrimers and polymeric nanoparticles [27–29,36,38–41]. Through the calculation of the fractal dimension, some interesting aggregation phenomena can be predicted, in order to better understand the physicochemical and morphological behaviour of nanoparticles, such as the self-assembled fractal growth of poly(amidoamine) (PAMAM) dendrimers in aqueous medium [40] or the polymeric growth process and kinetics of gold nanoparticle aggregation [41]. Moreover, Pippa et al. [27–29,38,39] also correlated the d_f with the self-assembly and the morphology of liposomes composed of lipids, as well as mixed polymeric-lipidic liposomal nanocarriers and elucidated their structural response, depending on the concentration and temperature, in different aqueous media. In the present work, the fractal dimension of the liquid crystalline nanosystems, is used to monitor their structural response to temperature and environmental pH changes. We should also mention that this is the first report in the literature, where fractal dimension parameter has been
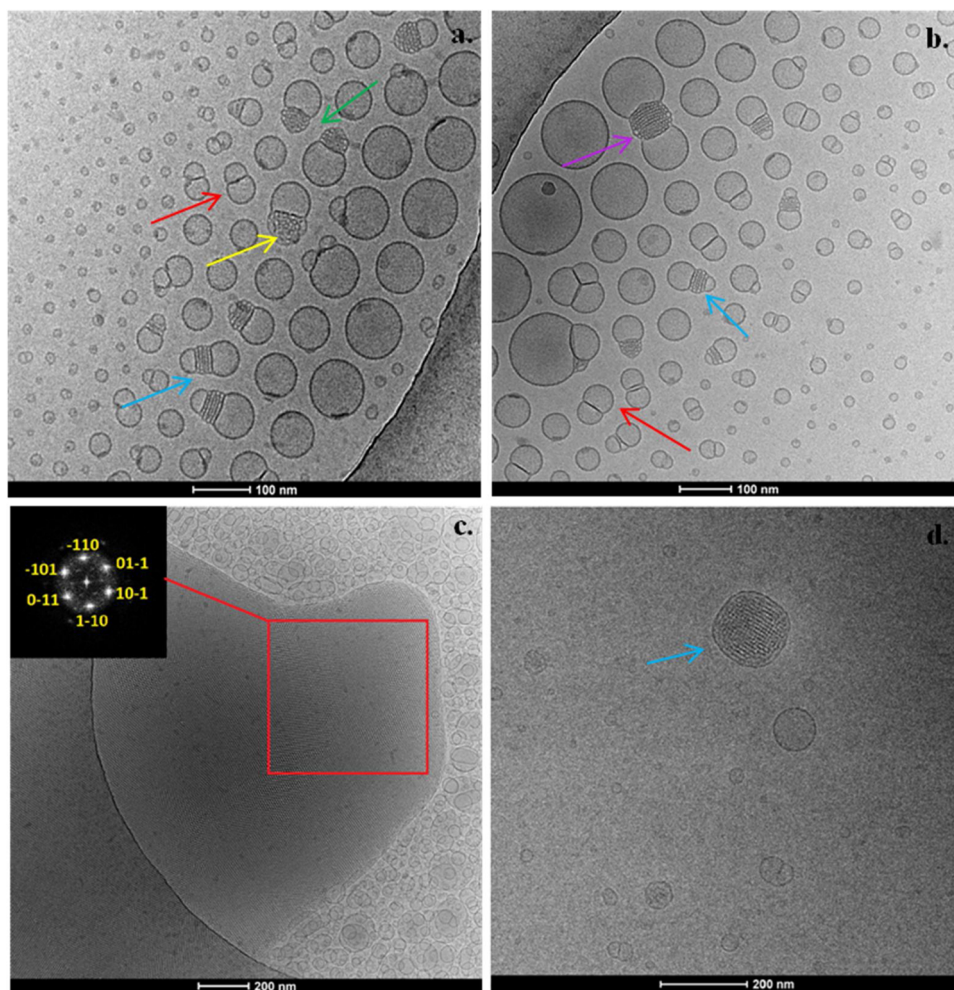
Fig. 4. Cryo-TEM images of GMO:PDMAEMA-b-PLMA 9:1 (**a-b**), GMO:PDMAEMA-b-PLMA:P407 8:1:1 (**c-d**) nanosystems. The corresponding Fast Fourier Transform (FFT) pattern of red box area (inset in image **c**) is likely with cubic structure of *Pn3m* symmetry. (For interpretation of the references to colour in this figure legend, the reader is referred to the web version of this article).

calculated, by exploiting SLS technique, in non lamellar liquid crystalline nanoparticles.

According to our results, the lipid and the polymer concentration affected the values of d_f of all the systems. In the cases of P407 stabilized nanoparticles (Table 2), the PHYT prepared nanosystems presented higher values of d_f, compared to the GMO ones. Regarding the systems containing the PDMAEMA-b-PLMA (Table 2), there were varying values of d_f, between GMO and PHYT-based systems.

The differentiation of the fractal dimension observed at the different lipid or polymer concentration can also be correlated with the observed morphological differences among the systems as revealed by cryo-TEM. Indeed, the higher values of d_f of PHYT systems, compared to GMO ones, can be correlated with the more compact, regularly ordered inner structure, as observed in PHYT systems (Fig. 3c, d).

Particularly, for the nanosystems stabilized with PDMAEMA-b-PLMA the calculated d_f values were lower than 2. The only exception was for the GMO:PDMAEMA-b-PLMA 9:1 system. In this case, the required acidification for this system yielded protonation of the polymeric amino side groups and increased hydrophilicity, maybe affecting its morphological conformation in a different manner, as reflected by the increased values of d_f being larger than 2.

Moreover, another significant observation was a decrease of d_f values upon temperature in the case of P407 stabilized nanosystems (Table 2), revealing a temperature induced structural re-conformation. Literature confirms that GMO and PHYT-based liquid crystalline nanosystems exhibit temperature-induced mesophases transitions at the

studied temperature range of $25-55\,°C$ [42,43]. Similarly, the decrease of d_f upon heating has been also observed for liposomes, a phenomenon that has been correlated with a heterogeneous microdomain structure on the lipid bilayer surface [27,28,44]. In more detail, as reported by the lipids phase diagram, while temperature increases, the self-assembled nanostructure changes showing increasing Gaussian curvature, *i.e.* the membrane becomes more curved [45,46]. Fong et al. [45,46] highlighted that this is attributed to the fact that the hydrophobic tail of the amphiphiles becomes more mobile and occupies a larger volume, changing the packing of the molecules, thus leading to the preference of surfaces with a higher Gaussian curvature. For example in the case of P407-stabilized PHYT particles, a formation of inverse micellar solution and disappearance of cubic phase were observed above $50\,°C$ [47]. In the case of GMO-prepared nanoparticles containing different fatty acids, as temperature increased, all nanoparticles gradually transformed from a micellar cubic phase *(Fd3m* phase) to an inverse microemulsion phase (L_2 phase) [46]. Our results show that as temperature increases, the d_f value decreases in the P407-stabilised systems of both GMO and PHYT lipids. This decrease of the d_f can be correlated with the temperature-induced transition to less compact structures or equally to more lamellar conformations, in line with the described increasing Gaussian curvature phenomena. Instead, not a clear relationship was observed between d_f values at the two investigated temperatures for the systems stabilized with PDMAEMA-b-PLMA (Table 2). Maybe, the temperature-responsive properties of the PDMAEMA block interfere in the temperature-induced structural re-conformation in a

Table 2

The fractal dimension d_f of the GMO- and PHYT-based nanosystems stabilized by P407 or PDMAEMA-b-PLMA at two different temperatures (25 °C, 55 °C) and as a function of pH (4.2 and 6.0).

Sample	Weight ratio	T (°C)	pH	d_f
PHYT:P407	9:1	25	6.0	2.84
		55		2.42
		25 (after cooling)		2.41
PHYT:P407	4:1	25	6.0	1.95
		55		1.77
		25 (after cooling)		*
GMO:P407	9:1	25	6.0	1.53
		55		1.42
		25 (after cooling)		1.45
GMO:P407	4:1	25	6.0	1.41
		55		1.25
		25 (after cooling)		*
PHYT:PDMAEMA-b-PLMA	9:1	25	4.2	1.33
			6.0	1.13
		55		1.34
		25 (after cooling)		1.78
PHYT:PDMAEMA-b-PLMA:P407	8:1:1	25	4.2	1.88
			6.0	1.38
		55		1.36
		25 (after cooling)		1.55
GMO:PDMAEMA-b-PLMA	9:1	25	4.2	*
			6.0	2.36
		55		1.96
		25 (after cooling)		2.12
GMO:PDMAEMA-b-PLMA:P407	8:1:1	25	4.2	1.93
			6.0	1.02
		55		1.05
		25 (after cooling)		0.98

All the data were obtained at the preparation day (t = 0 days) of the nanosystems.

  * not determined.

different way compared to the P407 stabilized nanosystems.

The d_f values for the PDMAEMA-b-PLMA stabilized nanosystems exhibit also a dependence on pH, probably due to the presence of the tertiary amine groups. We observed a d_f increase for all the systems stabilized with PDMAEMA-b-PLMA from pH 6 to pH 4.2 suggesting that the pH-responsiveness of PDMAEMA block has been transmitted also to the final nanosystems. A potential response of the nanoparticles to acidic conditions would be useful towards endosomal escape and targeted drug release, because endosome lumen exhibits pH values of 4.5–5.5 [15]. Taking into account the pH-responsiveness of the PDMAEMA block of PDMAEMA-b-PLMA copolymer, while the pH is decreasing, the amine group is becoming more protonated, causing a decrease in Gaussian curvature. As reported above for the different temperature conditions, this pH-induced change of the surface

curvature can also be correlated with structural re-arrangement. Namely, Fong et al. [46] described that in the case of monoolein nanoparticles containing fatty acids, the carboxylic acid headgroups deprotonate in increased pH values and acquire a negative charge. Thus, the repulsion of the headgroups, due to the charge, results in the decreased surface curvature and consequently to a phase transition from micellar cubic ($Fd3m$) phase to hexagonal (H_2) phase. According to our results, an increase in d_f value was reported in the case of decreasing pH, where the PDMAEMA-b-PLMA amine groups of the surface were charged, reflecting a possible pH-induced transition to morphologies with lower surface curvature. Therefore, we can highlight a consistent trend between the d_f and the changes of the Gaussian curvature. This indicates that the fractal analysis can be very useful, towards the monitoring of the alterations of Gaussian curvature and therefore of the morphology, in response to the environmental conditions, such as temperature and pH.

We should note that in this study, the first fractal analysis of non-lamellar liquid crystalline mesophases is presented. In particular, the use of fractal analysis by employing the SLS technique provides an *in situ* characterization of the nanoparticle morphology and understanding of the structure of nanoparticles being in dispersion state. The SLS is considered to be an inexpensive technique, which is able to offer, through fractal analysis, a rapid screening and also a quantification of the changes of nanoassemblies morphology under different environmental conditions, as well as for different formulation parameters.

3.3. Thermal behaviour of GMO and PHYT dispersions

The thermal behaviour of GMO- and PHYT- based dispersions in the presence of the two different polymeric stabilizers (P407 and PDMAEMA-b-PLMA) was evaluated by the combination of three techniques as microcalorimetry (Fig. 5), high-resolution ultrasonic spectroscopy (Fig. 6) and rheology (Fig. 7). Specifically, the interest was focused on the possible effect of the stabilizer on the sol-gel transition of lipids forming the planar bilayer of the prepared liquid crystalline dispersions. Microcalorimetry is a well-established technique to study thermal transitions of materials of different nature (*e.g.* polymers, proteins, peptides), including lipids [48,49]. This technique has been widely exploited for the characterization of phospholipid sol-gel transition in a large variety of liposomal dispersions [50], but not fully exploited for the investigation of the thermal phase transition of GMO and PHYT-based aqueous dispersions. White [51] has reported temperature-dependent structural changes in planar bilayer formed by GMO and dispersed in various alkane solvents using capacitance measurements. These transitions were found in the range $15-18$ °C and, later, confirmed by photon correlation and light scattering studies [52,53], but never reported using other techniques.

More recently, Efrat et al. [54] have reported thermograms for GMO-ethanol-water loaded with carbamazepine, coenzyme Q10,
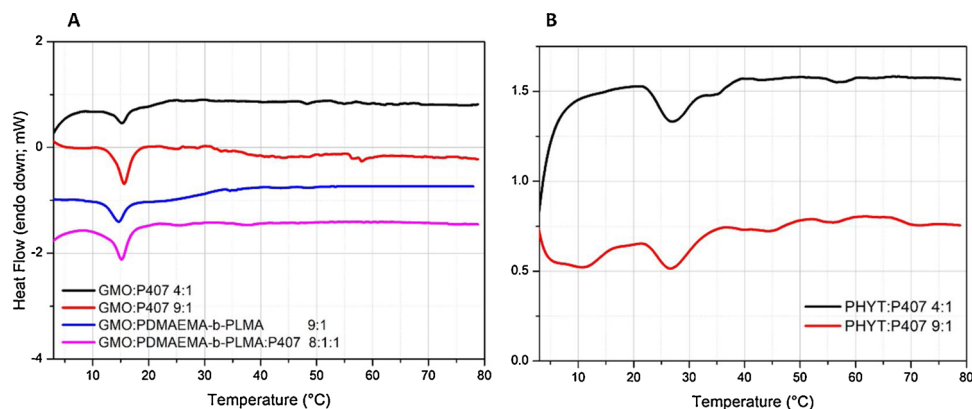

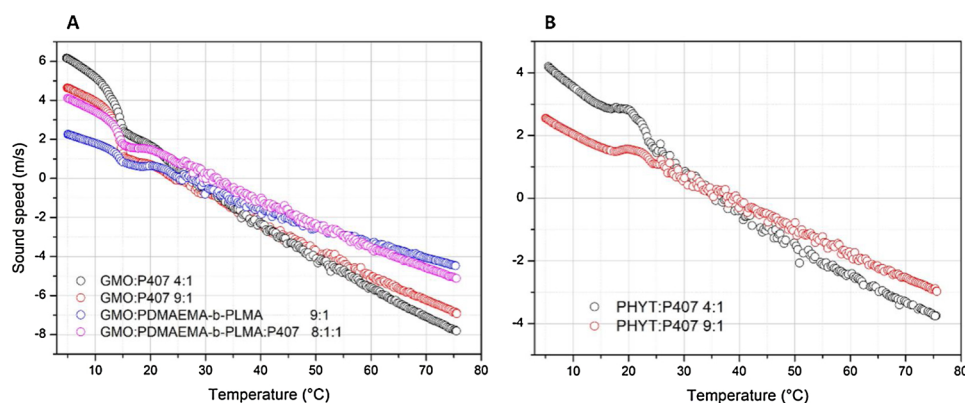**Fig. 5.** mDSC traces for GMO-based formulations (**A**) and for PHYT-based formulations (**B**).

Fig. 6. Sound speed *vs* temperature plots for GMO-based formulations (**A**) and for PHYT-based formulations (**B**).

cholesterol, or phytosterols, highlighting two thermal transitions, identified as the main transition of lipid bilayer from the lamellar L_β to the lamellar L_α mesophases. Moreover, at slightly higher temperature (approximately $12-13\,°C$ above the main transition), the transition to the so-defined discontinuous cubic mesophases (Q_L) was observed (L_α to Q_L). In another work, the lamellar to cubic phase transition of GMO-based aqueous systems loaded with model drugs was found in the range $30-40\,°C$ [55].

In our study, the obtained thermograms for GMO-based systems show a sharp endothermic transition centred in the range $14-16\,°C$, which can be attributed to the gel-to-sol main transition of the lipid (also referred as L_β to L_α) (Fig. 5). No appreciable differences in the main transition temperature have been observed between samples prepared using P407 or PDMAEMA-b-PLMA as stabilizer (Table 3). This result suggests a comparable interaction of the different stabilizers with lipid bilayer, which can be postulated by considering that the two amphiphilic copolymers (P407 and PDMAEMA-b-PLMA) have a comparable average molecular weight ($12,600\,g/mol$ *vs* $9,600\,g/mol$ and weight % of the hydrophobic portion 25.5% *vs* 30.3%). The possible interaction between P407 and GMO is not clearly understood, but as for phospholipid bilayers, the penetration of P407 into the bilayer, especially at a liquid crystalline state, can occur without markedly affecting the sol-gel transition [56,57].

Differently from GMO, no calorimetric data are available in the literature regarding the gel-to-sol main transition of PHYT and the only information about the phase behaviour is from X-rays diffraction or scattering studies [9,58]. We observed for PHYT dispersions a broader transition than GMO centered at around $26\,°C$, which it can be hypothesized to be the sol-gel transition of PHYT lipid bilayer. The formation of a cubic phase (L_α to Q_L transition) at a temperature higher than the lipid main transition is not unambiguously determined from the mDSC traces, due to the low concentration of the lipid in the dispersion.

From mDSC traces, also the enthalpy associated to the lipid main transition has been calculated (Table 3). No remarkable differences in enthalpy (J/g of solution) was observed among GMO-based nanosystems, independently from the amount and type of the stabilizer (P407, PDMAEMA-b-PLMA or both). On the other side, lower values were calculated for PHYT-based nanosystems, confirming that the energy associated to the main transition of studied nanosystems are dependent on the nature of the lipid used.

The transition temperatures can be also calculated from the other two techniques as high resolution-ultrasound (HR-US) and rheology. HR-US is a powerful technique to study the thermal transition of materials by following the variation over temperature of the two ultrasound parameters, sound speed and attenuation [59]. This technique has been successfully employed for the characterization of lipid nanovectors as liposomes and chimeric vesicles [49,60], but never applied for the characterization of cubosomal dispersions. Fig. 6 shows the variation of the sound speed for GMO-based and PHYT-based dispersions. Specifically, sound speed has a linear trend over temperature, but it shows a deviation as a stepwise decrease at the temperature around which the transition occurs. In all traces, the main transition of lipid is clearly detectable and main transition temperature values derived from HR-US were found comparable to those calculated by mDSC (Table 3).

Rheology is a technique already employed for the characterization of phase behaviour of liquid crystals. Generally, oscillatory measurements were performed on systems at a water content lower than 50% to follow how elastic (G') and viscous (G'') moduli change over temperature [61,62]. In this work, due to the lower consistency of the samples (liquid at room temperature), a viscometry test over temperature was performed. The main transition can be observed as a marked drop in the viscosity for both lipid-based dispersions (Fig. 7). Particularly, for GMO-based dispersions, viscosity decreases from
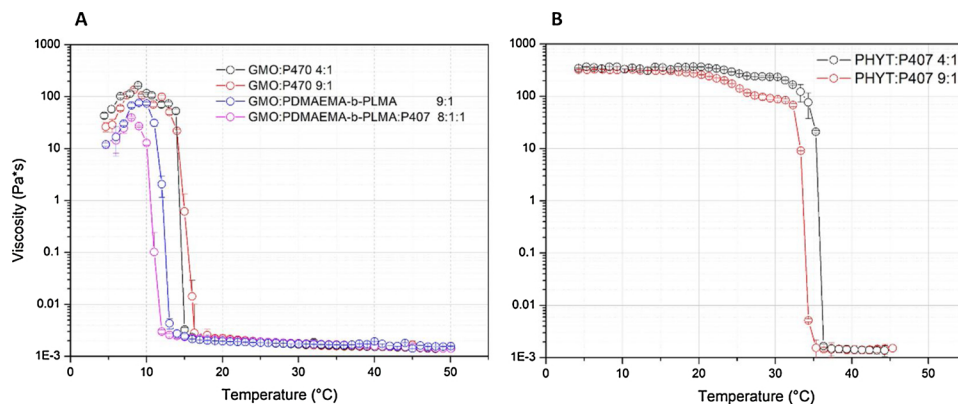

Fig. 7. Viscosity *vs* temperature plots (viscometry test) for the GMO-based formulations (**A**) and for the PHYT-based formulations (**B**).

Table 3

Thermodynamic parameters (transition temperature, ˚C and associated enthalpy, J/g of solution) for GMO- and PHYT-based formulations as calculated from microcalorimetry (mDSC), high-resolution ultrasound spectroscopy (HR-US) and rheology (viscometry test).

Sample	weight ratio	mDSC		HR-US (sound speed)	Rheology
		Transition temperature (˚C)	Enthalpy (J/g of solution)	Transition temperature (˚C)	Transition temperature (˚C)
GMO:P407	9:1	15.49 ± 0.15	0.132 ± 0.021	14.81 ± 0.12	14.46 ± 0.56
GMO:P407	4:1	15.46 ± 0.11	0.126 ± 0.022	14.67 ± 0.01	14.62 ± 0.41
GMO:PDMAEMA-b-PLMA	9:1	14.33 ± 0.15	0.130 ± 0.030	14.61 ± 0.14	12.09 ± 0.63
GMO:PDMAEMA-b-PLMA:P407	8:1:1	15.11 ± 0.13	0.161 ± 0.001	14.46 ± 0.25	11.02 ± 0.48
PHYT:P407	9:1	27.42 ± 0.22	0.073 ± 0.010	23.32 ± 0.21	23.52 ± 0.52*
					32.68 ± 0.63
PHYT:P407	4:1	26.44 ± 0.12	0.088 ± 0.004	23.78 ± 0.24	24.58 ± 0.46*
					33.24 ± 0.38

* The values were calculated by the two drops in viscosity for PHYT- based systems.

around 20–100 Pa*s to 10^{-3} Pa*s, as a consequence of the L_β to L_α transition. While for PHYT-based dispersions, the viscosity measured at temperatures below the transition was slightly higher (approximately 400 Pa*s). The drop in viscosity is sharper, occurring in a range of $2-3$ ˚C for GMO-based dispersions, while for PHYT-nanosystems it occurs in a large range of temperatures between 20 ˚C and 40 ˚C, reflecting the different broadness of the observed transition by calorimetry. For PHYT-based systems, a first decrease in viscosity (from around 400 Pa*s to 100 Pa*s) occurs before 30 ˚C but the large extent of dropping down to 10^{-3} Pa*s occurs between 30 ˚C and 40 ˚C. The calculated transition temperature values (Table 3) were comparable or slightly lower than those obtained from the other two techniques for GMO-based nanosystems. On the other side, two different temperatures were calculated for PHYT-based nanosystems from the two drops in viscosity. In this case, transition temperatures values from mDSC and HR-US were intermediate to those calculated from rheology, confirming the reasonable agreement of the results obtained from the three techniques.

4. Conclusions

Non-lamellar lipid liquid crystalline nanosystems from GMO and PHYT lipids were prepared and the stabilization efficiency of the alternative stimuli-responsive amphiphilic block copolymer PDMAEMA-b-PLMA was compared with this of the commonly used polymeric stabilizer P407. Firstly, PDMAEMA-b-PLMA block copolymer was effective as well as P407 in stabilizing the nanosystems prepared with GMO, without markedly affecting particle size distribution at least up to 40 days. PDMAEMA-b-PLMA was not effective, instead, for the stabilization of nanosystems prepared with PHYT, for which larger aggregates appeared after 3–5 days from preparation. Among the analyzed physicochemical properties, the presence of PDMAEMA-b-PLMA as stabilizer mainly affected ζ-potential and the fractal dimension (d_f parameter) of the liquid crystalline dispersion. Specifically, nanosystems prepared with PDMAEMA-b-PLMA yielded higher positive values of ζ-potential, probably due to the presence of charged amino groups in the copolymer, differently from nanosystems stabilized by P407 for which ζ-potential was negative. This aspect could be exploited for the development of cationic therapeutic nanosystems that will be able to get easily in complex with biological membranes and or macromolecules (e.g. nucleic acids) [15]. Fractal dimension parameter (d_f), being a useful tool for the morphological characterization of other categories of colloidal nanostructures [27–29,36,38–41], was calculated for the first time in the present report, for non-lamellar liquid crystalline nanoparticles from SLS data. Some differences have been highlighted as a function of the composition (including the different stabilizer used PDMAEMA-b-PLMA or P407). Moreover, this parameter was affected by temperature changes as well as by the alteration of the environmental pH, possibly reflecting a pH-responsive ability of nanosystem, due to the presence of the polycationic PDMAEMA-b-PLMA stabilizer.

Regarding the morphological characteristics, cryo-TEM revealed the presence of vesicles as well as nanoparticles with an internal structure, resembling cubic phases for GMO-based nanosystems, independently from the stabilizer used (PDMAEMA-b-PLMA or P407). In contrast, PHYT-based dispersions stabilized with P407 exhibited exclusively confined cubic liquid crystalline structures with absence of vesicles. Thermal behavior of GMO and PHYT liquid crystalline nanoparticles was studied for the first time, by the combination of microcalorimetry (mDSC), high-resolution ultrasound spectroscopy and rheology, while these methods have provided significant information in other categories of lipidic nanocarriers [49,50,60]. A different main transition temperature was observed between systems prepared with the two lipids, without any differences related to the stabilizers, probably due to their comparable interaction with the GMO lipid bilayer. In conclusion, in our report, for the first time, we performed a detailed characterization of the physicochemical, morphological and thermal behavior of non-lamellar lipidic liquid crystalline nanoparticles. The present study, continuing also our recently published work [63], proposes extra useful techniques, being applied for the first time at the liquid crystalline nanosystems, in order to upgrade the current methodologies for the characterization of this promising category of colloid nanostructures and deeply understand the interfacial phenomena taking place into their structure. Overall, taking into account that the non-lamellar lipidic liquid crystalline nanoparticles are nowadays gaining the momentum in the pharmaceutical nanotechnology field, all the information gathered in this study from the application of different techniques in terms of physicochemical, morphological and thermal characterization, is useful for the development of new and effective therapeutic nanosystems, belonging to this category of nanoparticles. Finally, their thorough evaluation is essential towards the achievement of safety and increased therapeutic efficiency.

CRediT authorship contribution statement

Maria Chountoulesi: Investigation, Visualization, Writing - original draft. **Diego Romano Perinelli:** Investigation, Visualization, Writing - original draft. **Natassa Pippa:** Investigation, Visualization, Writing - original draft. **Varvara Chrysostomou:** Investigation. **Aleksander Forys:** Investigation, Visualization, Writing - original draft. **Lukasz Otulakowski:** Investigation. **Giulia Bonacucina:** Writing - review & editing, Resources, Supervision. **Barbara Trzebicka:** Writing - review & editing, Resources, Supervision. **Stergios Pispas:** Writing - review & editing, Resources, Supervision. **Costas Demetzos:** Writing - review & editing, Resources, Supervision.

Declaration of Competing Interest

The authors declare that they have no known competing financial interests or personal relationships that could have appeared to influence the work reported in this paper.

Acknowledgements

Appendix A. Supplementary data

Supplementary material related to this article can be found, in the online version, at doi:https://doi.org/10.1016/j.colsurfa.2020.124678.

References

[1] S. Akbar, A. Anwar, A. Ayish, J.M. Elliott, A.M. Squires, Phytantriol based smart nano-carriers for drug delivery applications, Eur. J. Pharm. Sci. 101 (2017) 31–42.

[2] I.D. Azmi, S.M. Moghimi, A. Yaghmur, Cubosomes and hexosomes as versatile platforms for drug delivery, Ther. Deliv. 6 (12) (2015) 1347–1364.

[3] X. Mulet, B.J. Boyd, C.J. Drummond, Advances in drug delivery and medical imaging using colloidal lyotropic liquid crystalline dispersions, J. Colloid Interface Sci. 393 (2013) 1–20.

[4] H.M.G. Barriga, M.N. Holme, M.M. Stevens, Cubosomes: the next generation of smart lipid nanoparticles? Angew. Chem. Int. Ed. 58 (2019) 2958–2978.

[5] S. Urandur, D. Marwaha, S. Gautam, V.T. Banala, M. Sharma, P.R. Mishra, Nonlamellar liquid crystals: a new paradigm for the delivery of small molecules and bio-macromolecules, Ther. Deliv. 9 (9) (2018) 667–689.

[6] A. Lancelot, T. Sierra, J.L. Serrano, Nanostructured liquid-crystalline particles for drug delivery, Expert Opin. Drug Deliv. 11 (4) (2014) 547–564.

[7] A. Yaghmur, O. Glatter, Characterization and potential applications of nanostructured aqueous dispersions, Adv. Colloid Interface Sci. 147–148 (2009) 333–342.

[8] J. Gustafsson, H. Ljusberg-Wahren, M. Almgren, K. Larsson, Submicron particles of reversed lipid phases in water stabilized by a nonionic amphiphilic polymer, Langmuir 13 (1997) 6964–6971.

[9] Y.D. Dong, I. Larson, T. Hanley, B.J. Boyd, Bulk and dispersed aqueous phase behavior of phytantriol: effect of vitamin E acetate and F127 polymer on liquid crystal nanostructure, Langmuir 22 (2006) 9512–9518.

[10] J.Y.T. Chong, X. Mulet, A. Postma, D.J. Keddie, L.J. Waddington, B.J. Boyd, C.J. Drummond, Novel RAFT amphiphilic brush copolymer steric stabilisers for cubosomes: poly(octadecyl acrylate)-block-poly(polyethylene glycol methyl ether acrylate), Soft Matter 10 (2014) 6666–6676.

[11] J. Zhai, T.M. Hinton, L.J. Waddington, C. Fong, N. Tran, X. Mulet, C.J. Drummond, B.W. Muir, Lipid-PEG conjugates sterically stabilize and reduce the toxicity of phytantriol-based lyotropic liquid crystalline nanoparticles, Langmuir 31 (39) (2015) 10871–10880.

[12] J. Zhai, R. Suryadinata, B. Luan, N. Tran, T.M. Hinton, J. Ratcliffe, X. Hao, C.J. Drummond, Amphiphilic brush polymers produced using the RAFT polymerisation method stabilise and reduce the cell cytotoxicity of lipid lyotropic liquid crystalline nanoparticles, Faraday Discuss. 191 (2016) 545–563.

[13] W.K. Fong, R. Negrini, J.J. Vallooran, R. Mezzenga, B.J. Boyd, Responsive self-assembled nanostructured lipid systems for drug delivery and diagnostics, J. Colloid Interface Sci. 484 (2016) 320–339.

[14] M. Kluzek, A.I.I. Tyler, S. Wang, R. Chen, C. Marques, F. Thalmann, J. Seddon, M. Schmutz, Influence of a pH-sensitive polymer on the structure of monoolein cubosomes, Soft Matter 13 (2017) 7571–7577.

[15] M. Kanamala, W.R. Wilson, M. Yang, B.D. Palmer, Z. Wu, Mechanisms and biomaterials in pH-responsive tumour targeted drug delivery: a review, Biomaterials 85 (2016) 152–167.

[16] K. Kim, W.C.W. Chen, Y. Heo, Y. Wang, Polycations and their biomedical applications, Prog. Polym. Sci. 60 (2016) 18–50.

[17] S. Bazban−Shotorbani, M.M. Hasani−Sadrabadi, A. Karkhaneh, V. Serpooshan, K.I. Jacob, A. Moshaverinia, M. Mahmoudi, Revisiting structure-property relationship of pH-responsive polymers for drug delivery applications, J. Control. Release 253 (2017) 46–63.

[18] V. Chrysostomou, S. Pispas, Stimuli-responsive amphiphilic PDMAEMA-b-PLMA copolymers and their cationic and Zwitterionic analogs, J. Polym. Sci. Part A: Polym. Chem. 56 (6) (2018) 598–610.

[19] B. Mendrek, Ł. Sieroń, M. Libera, M. Smet, B. Trzebicka, A.L. Sieroń, A. Dworak, A. Kowalczuk, Polycationic star polymers with hyperbranched cores for gene delivery, Polymer 55 (18) (2014) 4551–4562.

[20] Z. Wang, X. Deng, J. Ding, W. Zhou, X. Zheng, G. Tang, Mechanisms of drug release in pH-sensitive micelles for tumor targeted drug delivery system: a review, Int. J. Pharm. 535 (1−2) (2018) 253–260.

[21] S. Agarwal, Y. Zhang, S. Maji, A. Greiner, PDMAEMA based gene delivery materials, Mater. Today 15 (9) (2012) 388–393.

[22] B. Mendrek, Ł. Sieroń, I. Zymełka−Miara, P. Binkiewicz, M. Libera, M. Smet, B. Trzebicka, A.L. Sieroń, A. Kowalczuk, A. Dworak, Nonviral plasmid DNA carriers based on N,N′-Dimethylaminoethyl methacrylate and di(ethylene glycol) methyl ether methacrylate star copolymers, Biomacromolecules 16 (10) (2015) 3275–3285.

[23] J. Mao, X. Ji, S. Bo, Synthesis and pH/Temperature-Responsive behavior of PLLA-b-PDMAEMA block polyelectrolytes prepared via ROP and ATRP, Macromol. Chem. Phys. 212 (2011) 744–752.

[24] E. Stubbs, E. Laskowski, P. Conor, D.A. Heinze, D. Karis, E.M. Glogowski, Control of pH- and temperature-responsive behavior of mPEG-b-PDMAEMA copolymers through polymer composition, J. Macromol. Sci. A 54 (4) (2017) 228–235.

[25] M. Demetriou, T. Krasia−Christoforou, Synthesis and characterization of well-defined block and statistical copolymers based on lauryl methacrylate and 2-(acetoacetoxy)ethyl methacrylate using RAFT-controlled radical polymerization, J. Polym. Sci. Part A: Polym. Chem. 46 (2008) 5442–5451.

[26] S.P. Akhlaghi, I.R. Ribeiro, B.J. Boyd, W. Loh, Impact of preparation method and variables on the internal structure, morphology, and presence of liposomes in phytantriol-Pluronic® F127 cubosomes, Collids Surf. B Biointerfaces 145 (2016) 845–853.

[27] N. Pippa, S. Pispas, C. Demetzos, The fractal hologram and elucidation of the structure of liposomal carriers in aqueous and biological media, Int. J. Pharm. 430 (2012) 65–73.

[28] N. Pippa, S. Pispas, C. Demetzos, The delineation of the morphology of charged liposomal vectors via a fractal analysis in aqueous and biological media: physicochemical and self-assembly studies, Int. J. Pharm. 437 (2012) 264–274.

[29] N. Pippa, F. Psarommati, S. Pispas, C. Demetzos, The shape/morphology balance: a study of stealth liposomes via fractal analysis and drug encapsulation, Pharm. Res. 30 (2013) 2385–2395.

[30] N. Pippa, E. Kaditi, S. Pispas, C. Demetzos, PEO-b-PCL/DPPC chimeric nanocarriers: self-assembly aspects in aqueous and biological media and drug incorporation, Soft Matter 9 (2013) 4073–4082.

[31] S.B. Rizwan, D. Assmus, A. Boehnke, T. Hanley, B.J. Boyd, T. Rades, S. Hook, Preparation of phytantriol cubosomes by solvent precursor dilution for the delivery of protein vaccines, Eur. J. Pharm. Biopharm. 79 (2011) 15–22.

[32] J. Barauskas, M. Johnsson, F. Joabsson, F. Tiberg, Cubic phase nanoparticles (Cubosome†): principles for controlling size, structure, and stability, Langmuir 21 (2005) 2569–2577.

[33] L. de Campo, A. Yaghmur, L. Sagalowicz, M.E. Leser, H. Watzke, O. Glatter, Reversible phase transitions in emulsified nanostructured lipid systems, Langmuir 20 (2004) 5254–5261.

[34] J.Y.T. Chong, X. Mulet, L.J. Waddington, B.J. Boyd, C.J. Drummond, Steric stabilisation of self-assembled cubic lyotropic liquid crystalline nanoparticles: high throughput evaluation of triblock polyethylene oxide-polypropylene oxide-polyethylene oxide copolymers, Soft Matter 7 (2011) 4768–4777.

[35] J.Y.T. Chong, X. Mulet, L.J. Waddington, B.J. Boyd, C.J. Drummond, High-throughput discovery of novel steric stabilizers for cubic lyotropic liquid crystal nanoparticle dispersions, Langmuir 28 (2012) 9223–9232.

[36] N. Pippa, A. Dokoumetzidis, C. Demetzos, P. Macheras, On the ubiquitous presence of fractals and fractal concepts in pharmaceutical sciences: a review, Int. J. Pharm. 456 (2013) 340–352.

[37] J. Gregory, Monitoring particle aggregation processes, Adv. Colloid Interface Sci. 147–148 (2009) 109–123.

[38] N. Pippa, M. Merkouraki, S. Pispas, C. Demetzos, DPPC:MPOx chimeric advanced Drug Delivery nanosystems (chi-aDDnSs): physicochemical and structural characterization, stability and drug release studies, Int. J. Pharm. 450 (2013) 1–10.

[39] N. Pippa, E. Kaditi, S. Pispas, C. Demetzos, DPPC/poly(2-methyl-2- oxazoline)-grad-poly(2-phenyl-2-oxazoline) chimeric nanostructures as potential drug nanocarriers, J. Nanopart. Res. 15 (2013) 1685.

[40] L. Metulio, M. Ferrone, A. Coslanich, S. Fuchs, M. Fermeglia, M.S. Paneni, S. Pricl, Polyamidoamine (yet not PAMAM) dendrimers as bioinspired materials for drug delivery: structure–activity relationships by molecular simulations, Biomacromolecules 5 (2004) 1371–1378.

[41] T. Kim, C.H. Lee, S.W. Joo, K. Lee, Kinetics of gold nanoparticle aggregation: experiments and modeling, J. Colloid Interface Sci. 318 (2008) 238–243.

[42] H. Qiu, M. Caffrey, The phase diagram of the Monoolein/Water system: metastability and equilibrium aspects, Biomaterials 21 (2000) 223–234.

[43] D.H. Kim, S. Lim, J. Shim, J.E. Song, J.S. Chang, K.S. Jin, E.C. Cho, A simple evaporation method for the large scale production of liquid crystalline lipid nanoparticles with various internal structures, ACS Appl. Mater. Interfaces 7 (36) (2015) 20438–20446.

[44] K. Vogtt, C. Joworrek, V.M. Garamus, R. Winter, Microdomains in lipid vesicles: structure and distribution assessed by small-angle scattering, J. Phys. Chem. B 114 (2010) 5643–5648.

[45] C. Fong, T. Le, C.J. Drummond, Lyotropic liquid crystal engineering–ordered nanostructured small molecule amphiphile self-assembly materials by design, Chem. Soc. Rev. 41 (3) (2012) 1297–1322.

[46] C. Fong, J. Zhai, C.J. Drummond, N. Tran, Micellar Fd3m cubosomes from monoolein − long chain unsaturated fatty acid mixtures: stability on temperature and pH response, J. Colloid Interface Sci. 566 (2020) 98–106.

[47] F. Muller, A. Salonen, O. Glatter, Phase behavior of Phytantriol/water bicontinuous cubic Pn3m cubosomes stabilized by Laponite disc-like particles, J. Colloid Interface Sci. 342 (2) (2010) 392–398.

[48] L. Signorello, S. Pucciarelli, G. Bonacucina, V. Polzonetti, M. Cespi, D.R. Perinelli, G.F. Palmieri, R. Pettinari, C. Pettinari, G. Fiorentini, S. Vincenzetti, Quantification, microbial contamination, physico-chemical stability of repackaged bevacizumab stored under different conditions, Curr. Pharm. Biotechnol. 15 (2) (2014) 113–119.

[49] D.R. Perinelli, M. Cespi, G. Bonacucina, F. Rendina, G.F. Palmieri, Heating treatments affect the thermal behaviour of doxorubicin loaded in PEGylated liposomes, Int. J. Pharm. 534 (1−2) (2017) 81–88.

[50] H. Heerklotz, The microcalorimetry of lipid membranes, J. Phys. Condens. Matter

16 (2004) 441–467.

[51] S.H. White, Phase transition in planar bilayer membranes, Biophys. J. 15 (1975) 95–117.

[52] G.E. Crawford, J.C. Earnshaw, Photon correlation spectroscopy as a probe of planar lipid bilayer phase transitions, Eur. Biophys. J. 11 (1984) 25–33.

[53] G.E. Crawford, J.C. Earnshaw, Phase transitions in monoglyceride bilayers. A light scattering study, Biophys. J. 49 (1986) 869–889.

[54] R. Efrat, A. Aserin, E. Kesselman, D. Danino, E.J. Wachtel, N. Garti, Liquid micellar discontinuous cubic mesophase from ternary monoolein/ethanol/water mixtures, Colloids Surf. A Physicochem. Eng. Asp. 299 (1–3) (2007) 133–145.

[55] S. Engström, L. Lindahl, R. Wallin, J. Engblom, A study of polar lipid drug systems undergoing a thermoreversible lamellar-to-cubic phase transition, Int. J. Pharm. 86 (2–3) (1992) 137–145.

[56] J.D. Castile, K.M.G. Taylor, G. Buckton, A high sensitivity differential scanning calorimetry study of the interaction between poloxamers and dimyristoylphosphatidylcholine and dipalmitoylphosphatidylcholine liposomes, Int. J. Pharm. 182 (1999) 101–110.

[57] J.D. Castile, K.M.G. Taylor, G. Buckton, The influence of incubation temperature and surfactant concentration on the interaction between dimyristoylphosphatidylcholine liposomes and poloxamer surfactants, Int. J. Pharm. 221 (1–2)

(2001) 197–209.

[58] J. Barauskas, T. Landh, Phase behavior of the phytantriol/water system, Langmuir 19 (2003) 9562–9565.

[59] G. Bonacucina, D.R. Perinelli, M. Cespi, L. Casettari, R. Cossi, P. Blasi, G.F. Palmieri, Acoustic spectroscopy: a powerful analytical method for the pharmaceutical field? Int. J. Pharm. 503 (1–2) (2016) 174–195.

[60] T.M. Taylor, P.M. Davidson, B.D. Bruce, J. Weiss, Ultrasonic spectroscopy and differential scanning calorimetry of liposomal-encapsulated nisin, J. Agric. Food Chem. 53 (2005) 8722–8728.

[61] R. Mezzenga, C. Meyer, C. Servais, A.I. Romoscanu, L. Sagalowicz, R.C. Hayward, Shear rheology of lyotropic liquid crystals: a case study, Langmuir 21 (2005) 3322–3333.

[62] G. Bonacucina, G.F. Palmieri, D.Q.M. Craig, Rheological and dielectric characterization of monoolein/water mesophases in the presence of a peptide drug, J. Pharm. Sci. 94 (11) (2005) 2452–2462.

[63] M. Chountoulesi, N. Pippa, V. Chrysostomou, S. Pispas, E.D. Chrysina, A. Forys, L. Otulakowski, B. Trzebicka, C. Demetzos, Stimuli-responsive lyotropic liquid crystalline nanosystems with incorporated poly(2-Dimethylamino ethyl methacrylate)-b-Poly(Lauryl methacrylate) amphiphilic block copolymer, Polymers 11 (9) (2019) 1400.